

Bandwidth-controlled Mott transition in κ -(BEDT-TTF)₂Cu[N(CN)₂]Br_xCl_{1-x}:

I. Optical studies of localized charge excitations

Daniel Faltermeier, Jakob Barz, Michael Dumm, and Martin Dressel*

1. *Physikalisches Institut, Universität Stuttgart, Pfaffenwaldring 57, 70550 Stuttgart Germany*

Natalia Drichko

1. *Physikalisches Institut, Universität Stuttgart, Pfaffenwaldring 57, 70550 Stuttgart Germany and
Ioffe Physico-Technical Institute Russian Academy of Science Politeknicheskaya 26, 194021 St.Petersburg, Russia*

Boris Petrov, Victor Semkin, and Rema Vlasova

Ioffe Physico-Technical Institute Russian Academy of Science Politeknicheskaya 26, 194021 St.Petersburg, Russia

Cécile Meziere and Patrick Batail

*Laboratoire CIMI, FRE 2447 CNRS-Université d'Angers,
Bât. K, UFR Sciences, 2 Bd. Lavoisier, 49045 Angers, France*

(Dated: September 10, 2018)

Infrared reflection measurements of the half-filled two-dimensional organic conductors κ -(BEDT-TTF)₂Cu[N(CN)₂]Br_xCl_{1-x} were performed as a function of temperature ($5 \text{ K} < T < 300 \text{ K}$) and Br-substitution ($x = 0\%, 40\%, 73\%, 85\%, \text{ and } 90\%$) in order to study the metal-insulator transition. We can distinguish absorption processes due to itinerant and localized charge carriers. The broad mid-infrared absorption has two contributions: transitions between the two Hubbard bands and intradimer excitations from the charges localized on the (BEDT-TTF)₂ dimer. Since the latter couple to intramolecular vibrations of BEDT-TTF, the analysis of both electronic and vibrational features provides a tool to disentangle these contributions and to follow their temperature and electronic-correlations dependence. Calculations based on the cluster model support our interpretation.

PACS numbers: 74.70.Kn, 71.30.+h, 74.25.Gz, 71.10.Hf

I. INTRODUCTION

The physics of strongly correlated electron systems is a very active field in solid-state science where the vicinity of Mott-insulating, magnetically ordered, and superconducting ground states is most intriguing. These effects are intensively studied for transition-metal oxides, in particular high-temperature superconductors, and organic conductors. It is extremely interesting that all of these materials show a similar competition between ordered antiferromagnetic and superconducting phases: this suggests common physics, while the chemistry of the compounds and the origin of the conducting electrons is different.^{1,2,3} These facts have initiated our investigation of the molecular conductors of the BEDT-TTF family as model compounds to study physics of correlated electrons close to the Mott transition in two dimensions.^{4,5}

In the κ -phase crystals, conducting layers of cationic bis-(ethylenedithio)tetrathiafulvalene (BEDT-TTF) molecules are separated by ‘charge-reservoir’ layers of monovalent anions. As depicted in Fig. 1, two BEDT-TTF^{+0.5} molecules form confacial dimers which can be considered as lattice sites; due to this dimerization the conduction band is half filled. The anion size sensitively influences the physical properties of the system very similar to the variation of pressure, since they define the spacing between the molecules (molecular sites) and thus

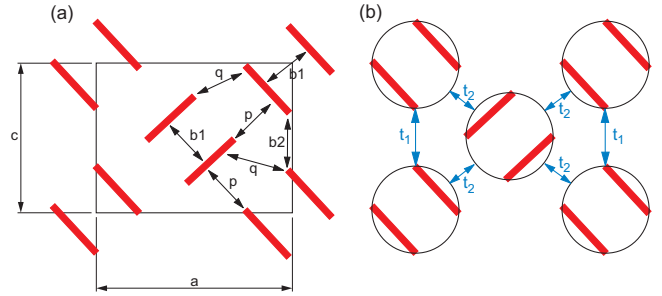


FIG. 1: (a) Structural arrangement of the BEDT-TTF molecules in the κ -phase (looking along the molecular axis); the size of the unit cell is approximately 12.9 \AA in a -direction, 8.5 \AA along the c axis, and 30.0 \AA in the third direction. The overlap integrals are labelled according to Mori *et al.* (Ref. 6). The interdimer overlap integral b_1 is around 0.027 , along the dimer chains $b_2 \approx 0.010$, while p and q link orthogonal molecules with approximately 0.011 and 0.004 , respectively. (b) Triangular lattice for the dimer model of κ -(BEDT-TTF)₂X. There is hopping along the stacks t_1 and along the diagonals t_2 .

the width of the band.^{6,7} The ratio of electronic correlations to the width of the conductance band is the control parameter³ in the phase diagram depicted in Fig. 2. The ground state of κ -(BEDT-TTF)₂X salts can be switched between an antiferromagnetic insulating, a superconducting, and a metallic state. These salts exhibit the highest

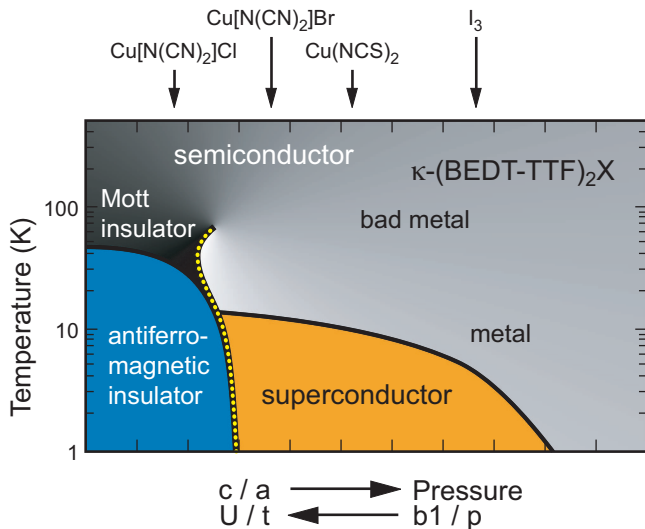


FIG. 2: Schematic phase diagram of the κ -phase salts (BEDT-TTF) $_2X$. Instead of tuning the external pressure, the same ambient-pressure ground state can be achieved by modifying the anions X . The arrows indicate the approximate position of κ -(BEDT-TTF) $_2$ Cu[N(CN) $_2$]Cl, κ -(BEDT-TTF) $_2$ -Cu[N(CN) $_2$]Br, κ -(BEDT-TTF) $_2$ Cu(NCS) $_2$, and κ -(BEDT-TTF) $_2$ I $_3$ at ambient pressure, respectively. The phase transition between the (antiferromagnetic) Mott insulator and the metal/superconductor can be explored by gradually replacing Cl by Br in κ -(BEDT-TTF) $_2$ Cu[N(CN) $_2$]Br $_x$ Cl $_{1-x}$. Here c and a are the lattice parameters; $b1$ and p indicate the transfer integral according to Fig. 1a. U/t is the on-site Coulomb repulsion with respect to the hopping integral t .

superconducting transition temperature of all organic superconductors with $T_c = 12.5$ K.^{1,2}

At ambient temperature the studied κ -phase BEDT-TTF salts have common properties, which may be characterized as a narrow-gap semiconductor or “bad metal”. When the temperature drops below a so-called coherence temperature $T_{\text{coh}} \approx 50$ K on the right side of the phase diagram, the metallic behavior becomes dominant due to the formation of Fermi liquid quasiparticles^{8,9} until a second-order transition occurs to a superconducting state. The nature of superconductivity in organic crystals is subject to discussion for twenty years¹⁰ but in the present study we focus on the metallic and insulating states. On the left side of the phase diagram (Fig. 2), i.e., for higher values of U/t , the system never shows metallic properties, but is gradually driven into an insulating state by electronic correlations as the temperature drops below 90 K; at $T_N \approx 35$ K magnetic order is observed. NMR measurements in deuterated samples κ -(d_8 -BEDT-TTF) $_2$ Cu[N(CN) $_2$]Br (which fall right on the phase boundary) revealed that at low temperatures the transition between the commensurate antiferromagnet and pseudogapped superconductor is of first order.¹¹ Most recently, enormous research efforts were dedicated to the metal-to-insulator transition and critical end-point in this highly correlated two-dimensional electron system.

The critical behavior in the vicinity of the Mott transition was investigated by dc measurements under external pressure and in magnetic field.^{12,13,14} The alloyed series κ -(BEDT-TTF) $_2$ Cu[N(CN) $_2$]Br $_x$ Cl $_{1-x}$, studied in the present work, covers the most interesting region of the phase diagram spanned by the pure Cl and Br salts, including the border between the Mott insulating and metallic phases. Our infrared reflection measurements of a series of compounds with Br concentration x varying between 0 and 90 % make it possible to explore the temperature and correlation (bandwidth)-dependent charge dynamics on crossing this phase boundary, as well as the unusual physical properties in the metallic region above the superconducting transition.

Several optical experiments were performed on the pristine compounds κ -(BEDT-TTF) $_2$ Cu[N(CN) $_2$]Br and κ -(BEDT-TTF) $_2$ Cu[N(CN) $_2$]Cl over the years.^{15,16,17,18,19,20,21} They gave a general idea of the electronic excitation observed in the infrared region: a broad mid-infrared band around 2500 – 3500 cm^{-1} and a narrow Drude-like peak in the spectra of superconducting Br-compound²² at temperatures below 50 K. In the discussion Section IV A we review the different interpretations of the mid-infrared spectra. Our investigation of the alloys gives an unambiguous assignment of the spectral features in this region, important for the analysis of the charge dynamics in these salts. BEDT-TTF) $_2$ Cu[N(CN) $_2$]Br $_{0.5}$ Cl $_{0.5}$ is the only mixed compound which has previously been investigated by infrared spectroscopy,^{19,23,24,25,26} but only in the mid-infrared range.

Here, we present for the first time a systematic optical study of the series κ -(BEDT-TTF) $_2$ Cu[N(CN) $_2$]Br $_x$ Cl $_{1-x}$, with x crossing all relevant regions of the phase diagram from the insulating/antiferromagnetic to the metallic/superconducting state. Our experiments cover a broad spectral range from 50 to 10000 cm^{-1} and temperatures from room temperature down to $T = 5$ K. This enables us to follow the response of the free and localized carriers for the different points of this phase diagram, depending on temperature and correlation-to-bandwidth ratio. While we focus on the signature of localized charge excitations here, the succeeding paper²⁷ (which we refer to as Part II in the following) is devoted to the dynamics of free charge carriers and the formation of the coherent quasiparticle response.

II. EXPERIMENTS

Single crystals of the κ -(BEDT-TTF) $_2$ Cu[N(CN) $_2$]Br $_x$ Cl $_{1-x}$ salts were grown by standard electrochemical methods. Certain ratios of Br/Cl concentration were chosen to obtain a series of alloys. Subsequent to the optical reflection experiments, each individual crystal was checked by microprobe analysis in order to determine the composition. The actual Br/Cl ratio turned out to be significantly different than expected from the starting con-

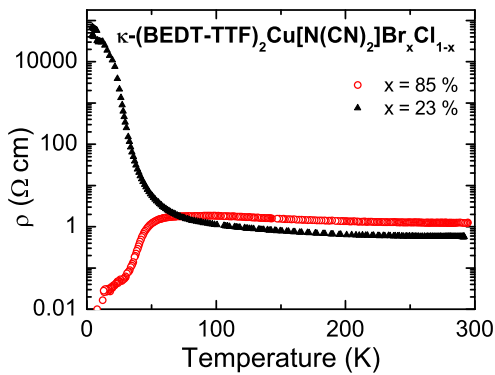


FIG. 3: Dc resistivity *versus* temperature of κ -(BEDT-TTF) $_2$ Cu[N(CN) $_2$]Br $_{0.23}$ Cl $_{0.77}$ and κ -(BEDT-TTF) $_2$ Cu[N(CN) $_2$]Br $_{0.85}$ Cl $_{0.15}$. While the latter compound becomes metallic below 100 K and eventually superconducting at $T_c = 12$ K, the former one gradually turns insulating.

centration, since Br enters the compounds much easier than Cl.²⁸ It was hardly possible to produce samples with predefined Br concentration. In the following, we denote the actual Br content of κ -(BEDT-TTF) $_2$ Cu[N(CN) $_2$]Br $_x$ Cl $_{1-x}$ where $x = 0\%$, 40% , 73% , 85% , and 90% ; the concentration was found homogeneous for each specimen. The platelets contained naturally flat (*ac*) surfaces with a typical size of about 1×1 mm 2 .²⁹ The orientation was determined from the optical spectra.

The strong dependence of the dc resistivity on the Br/Cl ratio is emphasized in Fig. 3 where $\rho(T)$ is plotted for a crystal with low ($x = 23\%$) and high ($x = 85\%$) bromine content. For the insulating sample κ -(BEDT-TTF) $_2$ Cu[N(CN) $_2$]Br $_{0.23}$ Cl $_{0.77}$ the resistivity rises by many orders of magnitude as the temperature decreases, most dramatically below 70 K. Contrary, κ -(BEDT-TTF) $_2$ Cu[N(CN) $_2$]Br $_{0.85}$ Cl $_{0.15}$ shows basically the same temperature dependence like the pure Br specimen: $\rho(T)$ increases slightly below room temperature until it reaches a broad maximum around 100 K. At lower temperatures the behavior is metallic with $\rho(T) \propto T^2$ for $T < 35$ K and finally a superconducting transition is observed at $T_c \approx 12$ K.³⁰ The superconducting properties of κ -(BEDT-TTF) $_2$ Cu[N(CN) $_2$]Br $_x$ Cl $_{1-x}$ with different Br concentrations have been investigated previously by dc resistivity and magnetization.³⁴

The in-plane optical reflectivity was measured with light polarized along *a* and *c* axes, respectively. Employing a modified Bruker IFS 113v Fourier-transform spectrometer, we covered a broad frequency range from 50 to 10000 cm $^{-1}$ (6 meV - 1.2 eV) with a resolution of up to 0.5 cm $^{-1}$. The single crystals were studied at 300, 150, 90, 50, 35, 20 and 5 K with the help of a cold-finger cryostat. To achieve good thermal contact, the samples were fixed by carbon paste on a brass cone directly attached to the cold finger. Absolute values of the reflectivity are obtained by subsequently evaporating gold onto the sample and remeasuring it as reference mir-

ror at all temperatures.³⁵ The *in-situ* gold-evaporation technique is more accurate than other referencing methods because it utilizes the entire sample surface and is less effected by surface imperfections. In addition, for the crystals with 40% and 85% Br concentration, reflectivity spectra were measured in 2000 – 12 000 cm $^{-1}$ range at temperatures between 300 and 20 K using a Bruker IFS 66v spectrometer equipped with an IR microscope and cold-finger Cryovac Microstat. The spectra in this range coincide for both methods of measurement; there is basically no dependence on Br-content and temperature. In the overlapping range they are in agreement with the room-temperature data received by Drozdova *et al.*²⁴ up to 40 000 cm $^{-1}$. These spectra were also used as a high-frequency extrapolation for the other compounds. From the reflectivity spectra, the optical conductivity was calculated employing Kramers-Kronig analysis.³⁶ At low-frequencies the data were extrapolated by the Hagen-Rubens behavior, which was double-checked by the dc resistivity obtained from standard four-probe measurements (Fig. 3). The low-frequency extrapolation only very weakly affects the spectra in the measured range, i.e. the absolute values of conductivity.

III. RESULTS

In Figs. 4 and 5 the reflectivity and conductivity spectra of κ -(BEDT-TTF) $_2$ Cu[N(CN) $_2$]Br $_x$ Cl $_{1-x}$ (with $x = 0\%$, 40% , 73% , 85% , and 90%) are plotted for light polarized parallel to the *a* direction at distinct temperatures from 300 K down to 20 K. Because there is no significant difference between the $T = 20$ K and 5 K spectra, we omitted the latter. At ambient temperature, the optical properties only weakly depend on the Br-content (inset of Fig. 4b). As expected for semiconductors, the reflectivity is basically frequency independent at small frequencies, and hence the corresponding room-temperature conductivity is low; the reflectivity starts to decrease significantly above 3500 cm $^{-1}$ and reaches a value close to zero in both polarizations around 5000 cm $^{-1}$. The respective conductivity spectra show a broad absorption band centered between 2000 cm $^{-1}$ and 3000 cm $^{-1}$ which is well documented in literature for the κ -phase of BEDT-TTF salts in general. The strong absorption features observed in the mid-infrared around 400, 850, and 1400 cm $^{-1}$ are totally symmetric vibrations of the BEDT-TTF molecule, activated by electron-molecular vibrational (emv) coupling (cf. Ref. 5 and references therein), we will give a detailed analysis in Sec. IV C.

Significant changes of the optical spectra are observed when cooling the samples below $T = 90$ K. The far-infrared reflectivity strongly increases for specimens with high Br content (Fig. 4), while the mid-infrared reflectivity is suppressed. Correspondingly, as seen in Fig. 5, a Drude-like contribution develops in the conductivity spectra of the samples with $x = 73\%$, 85% , and 90%

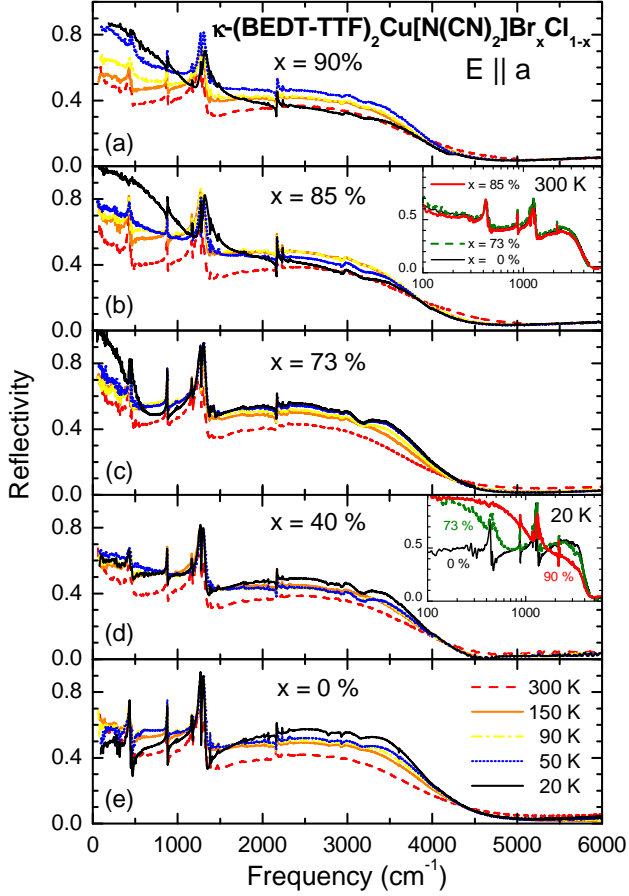


FIG. 4: Reflectivity spectra of κ -(BEDT-TTF) $_2$ Cu[N(CN) $_2$]Br $_x$ Cl $_{1-x}$ for the polarization $E \parallel a$ measured at various temperatures: $T = 300$ K, 150 K, 90 K, 50 K, and 20 K. The panels (a) - (e) correspond to different Br concentrations: $x = 90\%$, 85%, 73%, 40%, and 0%. The insets show the room-temperature and low-temperature spectra for $x = 90\%$, 73%, and 0% on a logarithmic frequency scale.

at low temperatures. The latter compound exhibits a behavior similar to the pristine κ -(BEDT-TTF) $_2$ Cu[N(CN) $_2$]Br salt.¹⁵ The opposite is observed for the salts with low Br-content: the far-infrared reflectivity drops while it rises in the mid-infrared. The absolute values of reflectivity and conductivity are slightly enhanced compared to previously published results.^{15,17,18,19,20,21} This we attribute to our advanced *in-situ* gold-evaporation method for the reference measurement which also accounts for imperfections of the crystal surface.

The reflectivity and conductivity for the perpendicular polarization ($E \parallel c$) are shown in Figs. 6 and 7 for different Br concentrations x and temperatures T . The spectra exhibit basically the same features as the ones recorded along a direction; except the shape of the mid-infrared absorption is different. As previously reported, for most other κ -salts, the maximum of the absorption band for the c axis lies at higher frequencies. While at ambient temperature a distinction is difficult, at low tem-

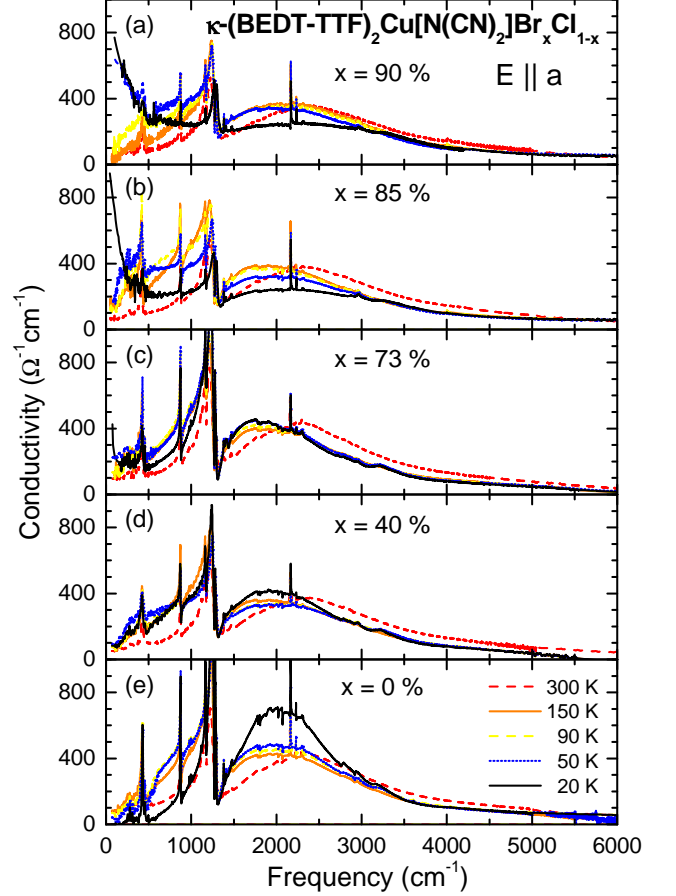


FIG. 5: Optical conductivity spectra ($E \parallel a$) of κ -(BEDT-TTF) $_2$ Cu[N(CN) $_2$]Br $_x$ Cl $_{1-x}$ at different Br concentrations x and temperatures, obtained by a Kramers-Kronig analysis from the data of Fig. 4.

peratures it becomes obvious from both, reflectivity and conductivity data, that it consists of two components: in addition to the band around 2000 cm^{-1} , a second narrower mode has its maximum around 3500 cm^{-1} . This behavior is most pronounced for the pure Cl compound. Again, with increasing Br content a Drude contribution develops as the temperature is reduced below 50 K.

We want to point out that the accessible frequency range of our experiments is limited to $\nu \geq 50 \text{ cm}^{-1}$ due to the small sample surfaces. Thus, we cannot detect the superconducting energy gap Δ_0 , which is expected around $2\Delta_0 = 3.53k_B T_c \approx 30 \text{ cm}^{-1}$.

IV. DISCUSSION

Despite the above mentioned limitations, our data cover a very broad frequency range from 50 to 10 000 cm^{-1} . Therefore, we are able not only to study the vibrational features and the mid-infrared absorption, but also to analyze the temperature and doping dependence of the Drude contribution in κ -(BEDT-TTF) $_2$ Cu-

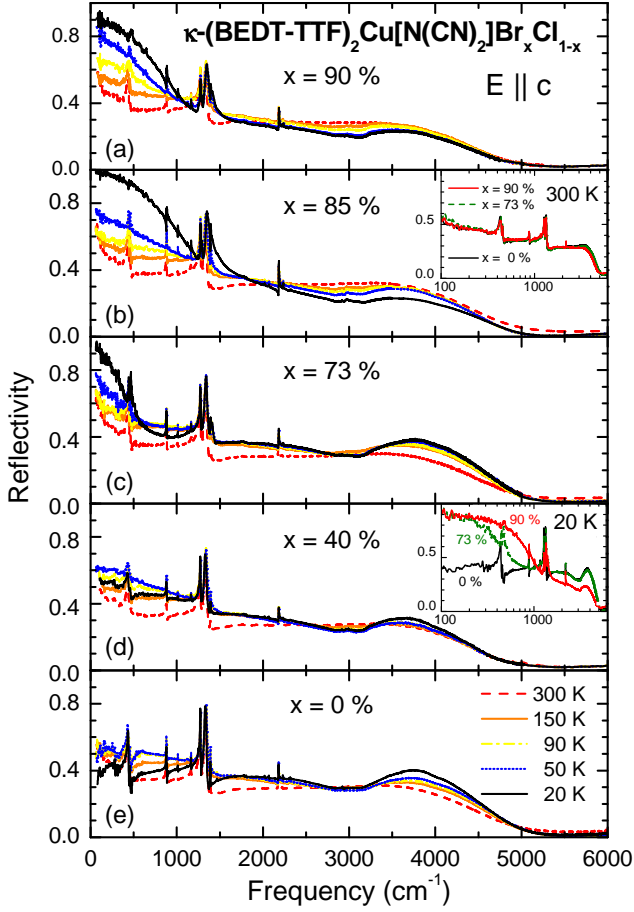


FIG. 6: Reflectivity spectra of κ -(BEDT-TTF) $_2$ Cu[N(CN) $_2$]Br $_x$ Cl $_{1-x}$ for light polarized $E \parallel c$ measured at various temperatures as indicated. The different panels (a) - (e) correspond to Br concentrations: $x = 90\%$, 85% , 73% , 40% , and 0% . The insets show the room-temperature and low-temperature spectra on a logarithmic frequency scale.

[N(CN) $_2$]Br $_x$ Cl $_{1-x}$. However, since there is no agreement in the literature on the interpretation of the mid-infrared absorption band which is important for analysis of the whole charge dynamics in these materials, we first address this part of the spectra. The contribution of the itinerant electrons will extensively be analyzed and discussed in Part II.

The common approach is to fit the spectra by the Drude-Lorentz model,^{5,36} because it helps to disentangle the contributions of conduction electrons, interband transitions and vibrational features. As an example, the optical conductivity along the c -direction of the crystal with $x = 0.85$ is displayed in Fig. 8 together with a fit by one Drude-like component and several Lorentzian oscillators; to further restrict the parameters, the $R(\omega)$ and $\sigma(\omega)$ spectra were fitted simultaneously. This procedure was applied to the spectra taken in both polarization directions and at all temperatures and values of Br doping.

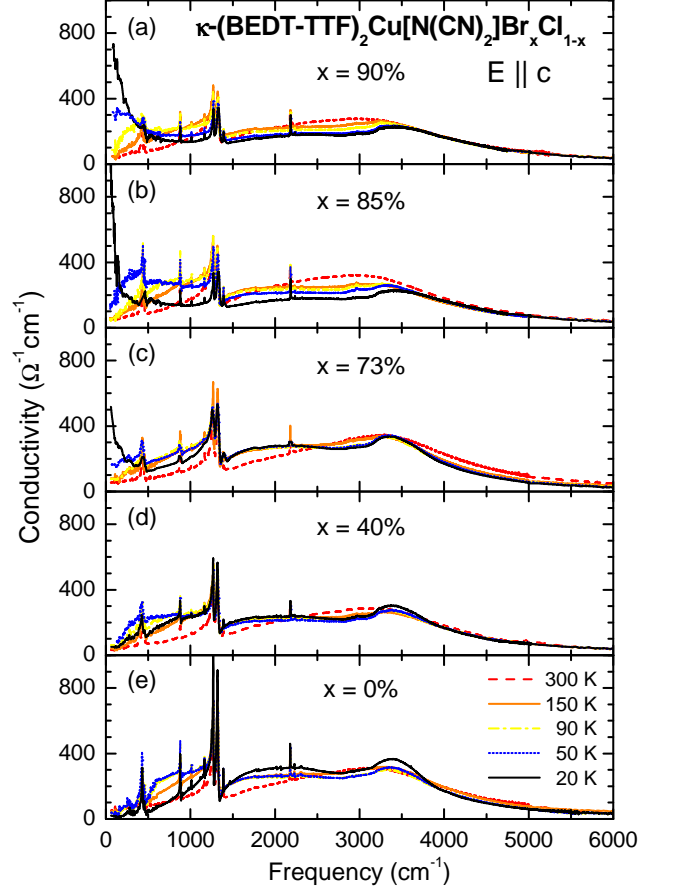


FIG. 7: Optical conductivity spectra ($E \parallel c$) for κ -(BEDT-TTF) $_2$ Cu[N(CN) $_2$]Br $_x$ Cl $_{1-x}$ of different Br concentrations (a) $x = 90\%$, (b) 85% , (c) 73% , (d) 40% , and (e) 0% measured at various temperatures: $T = 300$ K, 150 K, 90 K, 50 K, and 20 K. The mid-infrared band clearly has two contributions.

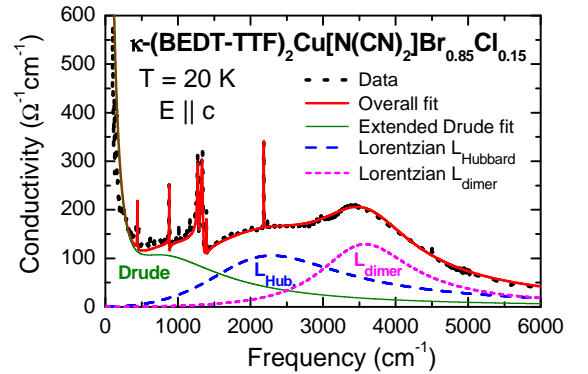


FIG. 8: Fit of the frequency dependent conductivity of κ -(BEDT-TTF) $_2$ Cu[N(CN) $_2$]Br $_{0.85}$ Cl $_{0.15}$ at 20 K for the electric field polarized parallel to the c axis. L_{dimer} and L_{Hubbard} show the two Lorentz oscillators required to fit the mid-infrared peak. The narrow lines describe the vibrational features. In addition an extended Drude model is included for the low-frequency increase.

A. Mid-Infrared band: overview of the different interpretations

In general, the most prominent feature in the optical conductivity spectra of κ -phase BEDT-TTF salts is the broad mid-infrared hump. It peaks around 2200 cm^{-1} for the polarization $E \parallel a$ and at 3200 cm^{-1} in the c direction, where it exhibits a more complicated double structure. Albeit it seems obvious – in particular when cooling down – that two contributions add up for this band, the explanations proposed over the years took into account only one single process. It was suggested that the mid-infrared peak is due to charge transfer inside the dimer^{15,16,17,37,46} or due to transitions between the Hubbard bands formed by the correlated conduction electrons.^{21,47,48}

Eldridge and coworkers^{15,17} first suggested that the mid-infrared peak is due to charge-transfer bands with the excitations confined to the dimers and the charge transfer occurring between adjacent molecules. The polarization dependence is explained by different interactions between neighboring dimers (Fig. 1a). The arguments were supported by electronic band-structure calculations of the κ -phase salts performed by Whangbo and collaborators on the basis of the tight-binding approximation.^{49,50} The highest occupied band is half filled with only very little difference in bandwidth and density of states at the Fermi level when going from κ -(BEDT-TTF)₂Cu[N(CN)₂]Cl to κ -(BEDT-TTF)₂Cu[N(CN)₂]Br. Obviously this is a very rough approximation which can explain neither the semiconducting behavior at ambient temperature, nor a redistribution of the spectral weight from this mid-infrared maximum to the Drude-peak for compounds with high Br concentration on cooling (discussed in Part II), nor the different ground states of the compounds.

A more consistent picture was achieved when both components of the optical conductivity, the Drude-like contribution and the mid-infrared hump were explained in the framework of a half-filled two-dimensional system with strong electronic correlations.^{4,6,51} The structure of the κ phase was mapped on an anisotropic triangular lattice, each site presenting one dimer as depicted in Fig. 1b. The interdimer overlap integrals define the hopping t between the sites of a triangular half-filled lattice considered by theory, they are $t_1 = 30\text{ meV}$ and $t_2 = 50\text{ meV}$.^{4,51} The intradimer overlap plays the role of the effective on-site Coulomb interaction U_{eff} .^{6,51,52} Consequently, U_{eff} increases with dimerization: for the Cl-analog b1 is slightly higher which causes larger U_{eff} . *Ab-initio* calculations by Fortunelli and Painelli⁵³ give the value of $U_{\text{eff}} = 0.4\text{ eV}$ for a dimer in κ -(BEDT-TTF)₂-Cu[N(CN)₂]Br; this is in agreement with experiments.

It has been predicted by theory that the Mott-insulator transition in a two-dimensional lattice typically occurs when U is comparable to the bandwidth $W = 8t$. In the present case $U_{\text{eff}}/t \approx 8$, implying that we are very close to the metal-insulator transition. U_{eff}/t increases

when going from Br to Cl anions, i.e. moving from right to left in the phase diagram (Fig. 2) and leads to localization of the charge carriers.⁵⁴ Following these considerations, recently²¹ the experimentally observed mid-infrared band around 3000 cm^{-1} was associated with the transition between the Hubbard bands at $\hbar\omega \approx U_{\text{eff}}$.

The application of dynamical mean-field theory to the metallic side of the phase diagram suggests^{9,48} that besides the mid-infrared band around U_{eff} , a quasiparticle peak at the Fermi level grows with temperature below $T_{\text{coh}} \approx 0.1t^*$, where t^* is the overlap integral. Due to transitions between the coherent quasiparticle band and the Hubbard bands, a new peak is supposed to develop around $\hbar\omega \approx U_{\text{eff}}/2$ for $T < T_{\text{coh}}$.

B. Mid-Infrared band: our experimental results

Our present investigation of the substitution series κ -(BEDT-TTF)₂Cu[N(CN)₂]Br_{*x*}Cl_{1-*x*} sheds new light on the above formulated controversy because all features were traced when going from the metallic to the insulating phase both by changing temperature T and the relative correlation strength U/t . This enabled us to disentangle the components coming from charge transfer inside the (BEDT-TTF)₂ dimers and between the dimers. We propose that the intradimer transitions cause the high-frequency contribution L_{dimer} , while the band L_{Hubbard} at lower frequencies is ascribed to interdimer transitions, i.e., to the transitions between the Hubbard bands.

Generally, the band of the intradimer transition is expected to appear at higher frequencies compared to the transition between the dimers. It was already shown for molecular chains that the high-frequency band vanishes when the dimerization is reduced;⁶⁰ calculations were also performed on a two-dimensional κ -like structure leading to similar conclusions.⁶¹ The same result is obtained by the cluster model,⁵⁸ when extending it to tetramers and hexamers; the electronic transitions summing up the intradimer and interdimer excitations shift to lower frequencies and get broader compared to the pure intradimer one.

In both reflectivity and conductivity spectra (Figs. 6 - 8) for light polarized parallel to the c axis, two bands can be clearly distinguished: a narrow high-frequency peak L_{dimer} and a broad peak L_{Hubbard} located at lower frequencies. Contrary, in a -direction there is no clear separation visible between L_{dimer} and L_{Hubbard} in the optical spectra (Figs. 4 and 5). Such an anisotropy in the mid-infrared range is well documented for these κ -salts.^{5,55} However, the detailed analysis based on the cluster model given below will show that despite the anisotropy both peaks are present in either orientations.

The temperature dependence of the L_{dimer} frequency ($E \parallel c$) is plotted in Fig. 9 for different Br concentrations. Within the uncertainty of the Lorentz fit, at ambient temperature the position of the high-frequency oscillator

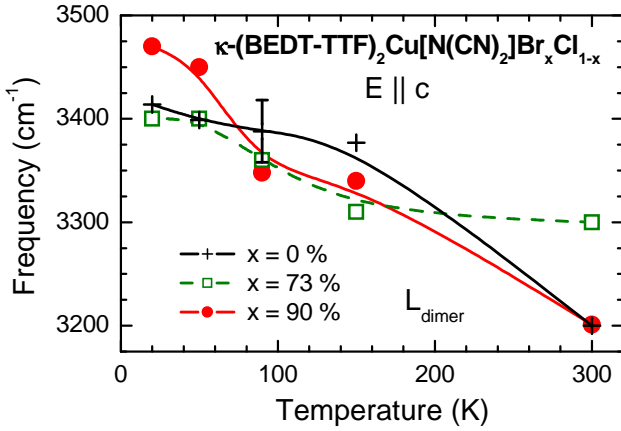


FIG. 9: Temperature dependence of the mid-infrared peak L_{dimer} in $\kappa\text{-(BEDT-TTF)}_2\text{Cu}[\text{N}(\text{CN})_2]\text{Br}_x\text{Cl}_{1-x}$ with $x = 0\%$, 73% , and 90% obtained by a Lorentzian fit for the polarization $E \parallel c$. The lines are guides to the eye.

L_{dimer} does not show a distinct dependence on the Br content along the c axis; also the oscillator strength of this band does not vary substantially. In general there is an upward shift of approximately 100 to 200 cm^{-1} when going down to $T = 20$ K. We attribute this blue shift to the thermal contraction of the single crystals which slightly enhances the intradimer transfer integral b_1 (Fig. 1a), i.e. the intradimer overlap increases⁶. The difference between metallic and insulating compounds is seen at 50 K and lower: while the temperature dependent high-frequency shift of L_{dimer} is more enhanced upon cooling in the metallic samples with $x = 90\%$ and 85% , it levels off for the insulating ones with low Br concentration. Obviously, the L_{dimer} oscillator frequency is not considerably affected by the opening of the Mott-Hubbard gap at $T \leq 50$ K which results in an increase of the dc resistivity of several orders of magnitude.

The intradimer transition, i.e., a charge transfer between the two face-to-face arranged BEDT-TTF molecules is expected to be strongly coupled to the totally symmetric molecular vibrations. Thus an detailed analysis of the experimentally obtained temperature dependence of their spectra and a comparison to the theoretical predictions of the cluster model will be the key to a final assignment of the electronic features in the spectra.

C. Vibrational features

The sharp absorption features in the frequency range between 400 cm^{-1} and 1600 cm^{-1} are known to be totally-symmetric vibrations activated by coupling with electronic excitations. In the course of numerous vibrational studies on the κ -phase BEDT-TTF salts, El-dridge's group^{18,37,38,39} and others^{20,24} presented a complete assignment of the totally-symmetric vibrations.

Here we use the C_{2h} symmetry assignment which takes a deformation of a BEDT-TTF molecule inside the crystal into account.⁴⁰ In our work we could follow not only the temperature, but also the doping-dependence of these features, that improves our interpretation of the spectra.

The most prominent $\nu_4(A_g)$ vibration involves a symmetric stretching of the C=C double bonds;⁵⁶ at room temperatures it is observed at about 1240 cm^{-1} along the a -axis and at 1280 cm^{-1} along the c -axis in the spectra of the $\kappa\text{-(BEDT-TTF)}_2\text{Cu}[\text{N}(\text{CN})_2]\text{Br}_x\text{Cl}_{1-x}$. We estimate the center frequency of the $\nu_4(A_g)$ band by fitting it with a Lorentzian, disregarding the anti-resonances due to the $\nu_6(A_g)$ mode for a moment. As can be seen from Fig. 11a and c, with decreasing temperature (300 K $\leq T < 50$ K) the $\nu_4(A_g)$ modes slightly shift to higher frequencies in about the same manner for all compounds. As T is reduced this tendency enhances further for $x = 85\%$ and 90% : the total shift amounts to approximately 45 cm^{-1} for $E \parallel a$, and less than 5 cm^{-1} in c direction; the variation saturates at very low temperatures. For the insulating compounds with low Br content, the $\nu_4(A_g)$ mode even reverses its temperature dependence below $T_{\text{coh}} \approx 50$ K and becomes softer. Except some gradual difference, the behavior is very similar for both orientations. Below 50 K, the $\nu_4(A_g)$ mode becomes sharper in the insulating samples while it broadens and seems to be weaker for high Br content.

The frequency of the $\nu_6(A_g)$ mode (vibration of the CH_2 groups) overlaps with the broad emv-coupled $\nu_4(A_g)$ band. In Fig. 10 the excitation is seen as an antiresonance around 1270 to 1280 cm^{-1} for $E \parallel a$ and slightly higher for the perpendicular direction. At low temperatures, four bands of $\nu_6(A_g)$ are resolved, originating from four distinct CH_2 groups per unit cell. We follow the temperature dependence by choosing the minimum around 1273 cm^{-1} . Again, for low Br content the $\nu_6(A_g)$ mode gradually moves down in frequency with decreasing temperature, while it significantly shifts to higher values for $x = 85\%$ and 90% as presented in Fig. 11c. The same temperature dependence of $\nu_6(A_g)$ is observed parallel to c (Fig. 11d). A similar temperature and Br-concentration dependence is seen for the peaks of the emv-coupled 'ring-breathing' mode $\nu_{10}(A_g)$ of the BEDT-TTF molecule⁴⁵ at 870 cm^{-1} and 885 cm^{-1} and of the $\nu_{13}(A_g)$ at about 430 cm^{-1} . Accordingly, the peaks are pretty intense in the insulating state, and are less significant in the spectra for high Br concentration.

In contrast to the emv-coupled modes, the infrared active $\nu_{45}(B_{2u})$ vibration of BEDT-TTF molecule detected around 1383 cm^{-1} (Fig. 10) and CN-stretch vibration of the anion layer observed around 2160 cm^{-1} do not depend on the Br-concentration and show no pronounced temperature dependence besides the expected hardening with cooling. Therefore, since the charge on the BEDT-TTF molecules is not redistributed in $\kappa\text{-(BEDT-TTF)}_2\text{Cu}[\text{N}(\text{CN})_2]\text{Br}_x\text{Cl}_{1-x}$ when the samples are cooled down, the characteristic temperature dependence of the emv-coupled A_g modes has to be due to the electronic excita-

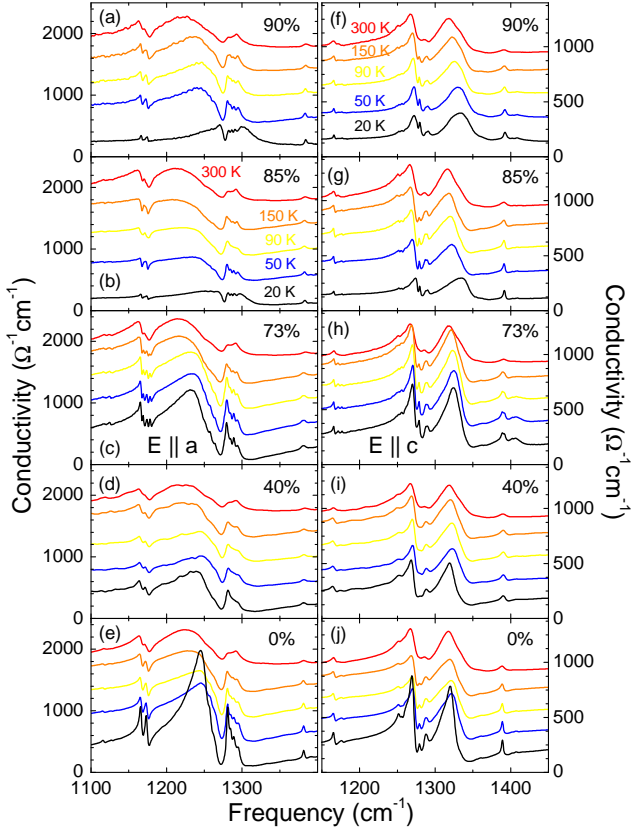


FIG. 10: Detailed view of the optical conductivity of κ -(BEDT-TTF) $_2$ Cu[N(CN) $_2$]Br $_x$ Cl $_{1-x}$ along the a and c -directions (left and right panels, respectively) for different Br concentrations $x = 90\%$, 85% , 73% , 40% , and 0% , (a)-(e) and (f)-(j), respectively. The spectra for the different temperatures (bottom to top: $T = 20$ K, 50 K, 90 K, 150 K, and 300 K) are offset by $400 (\Omega\text{cm})^{-1}$ for clarity.

tion to which they are coupled.

D. Excitations localized on dimers: charge transfer and emv-coupled features

The cluster model of M.J. Rice⁵⁷ and Delhaes and Yartsev^{58,59} describes the optical properties of molecular clusters with arbitrary geometry and equilibrium charge density distribution. The model describes optically activated charge transfer between the molecules in a cluster, the parameters defining this transition are transfer integral t between the molecules and Coulomb repulsion U_{mol} of two electrons on one molecule. In addition, this model takes into account an activation of totally symmetric vibrations by this charge transfer in a cluster; the strength of this coupling is defined by the coupling constants Q_i , specific for each given molecular vibration. It gives a correlation between a charge transfer electronic transition and the emv-coupled features. The vibrational modes become infrared active by emv coupling to

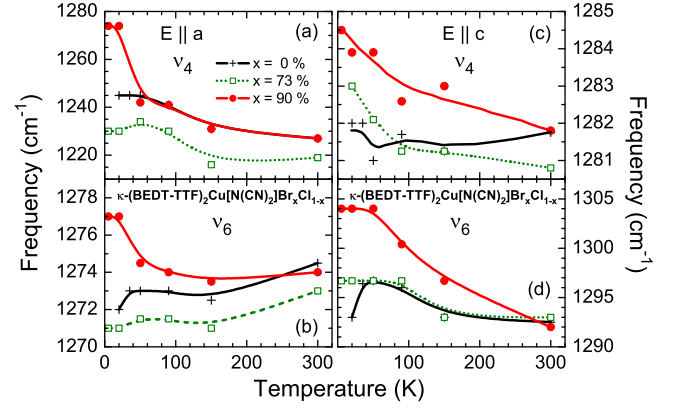


FIG. 11: Temperature dependence of the mode frequencies of the intramolecular vibrations $\nu_4(A_g)$ and $\nu_6(A_g)$ for κ -(BEDT-TTF) $_2$ Cu[N(CN) $_2$]Br $_x$ Cl $_{1-x}$ with Br concentrations 0% , 73% , and 90% . (a) The $\nu_4(A_g)$ mode along the a -direction was fitted by a Lorentzian and the center frequency plotted. (b) In the case of $\nu_6(A_g)$ the frequencies are defined as the minima in the respective optical conductivity, i.e. the strongest of the quadruple. In frames (c) and (d) the equivalent data are presented for the polarization $E \parallel c$. The lines correspond to spline fits.

the charge-transfer excitation; and they are shifted down in frequency with respect to the corresponding Raman modes.^{18,38,39} The shift and the intensity of the emv-coupled features depend on the coupling constants and on the position of the respective charge-transfer band. The model taking into account two perpendicular dimers of BEDT-TTF molecules successfully describes the mid-infrared peak and emv-coupled features in the room-temperature spectra of the κ -phase salts,^{58,62} while it does not account for the metallic behavior; thus it is not able to mimic the appearance of a Drude-peak in the compounds with high Br content.

In this work we use the simplest dimer model to describe the emv-coupled features present also in the metallic phase, and to verify the assignment of the mid-infrared peak L_{dimer} to the interdimer charge transfer. As an example, in Fig. 12a we show a fit by the dimer model of the 85% Br compound spectra. For $E \parallel c$ the dimer model with $U_{\text{mol}} = 0.5$ eV and transfer integral term $t(b1) = 0.21$ eV can reasonably well predict both the position of the high-frequency electronic maximum L_{dimer} and of the emv-coupled features. The value of the transfer integral energy is somewhat lower than those received by the Hückel method: $t(b1) = 0.26 - 0.27$ eV.^{4,6} Taking into account the very different approaches of these methods, the agreement is quite good. The differential spectrum of the experimentally obtained conductivity and the calculations by the dimer model shows that the intradimer transition is responsible for nearly all the intensity of the emv-coupled features. With other words, in the low-temperature metallic state the intradimer transition interacts strongly with the totally symmetric vibrations, while this process is less important for the charge

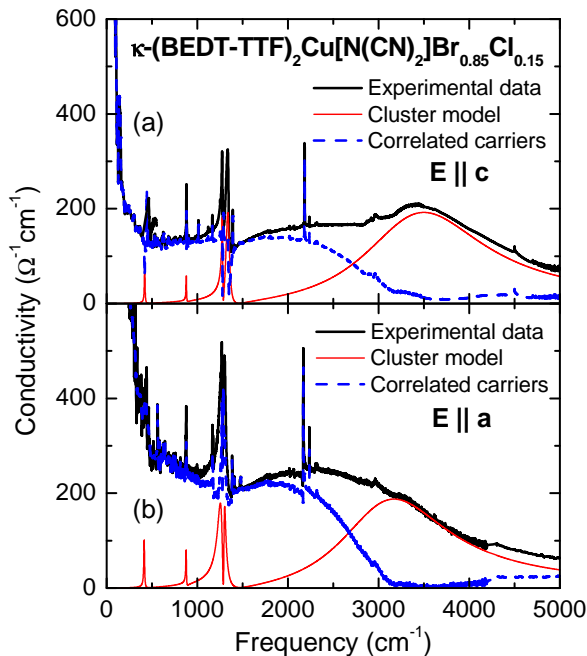


FIG. 12: Conductivity of κ -(BEDT-TTF)₂-Cu[N(CN)₂Br_{0.85}Cl_{0.15}] for the two polarizations (a) $E \parallel c$ and (b) $E \parallel a$ at $T = 20$ K. The solid red curves represent the conductivity for the intradimer transition and the emv coupled modes calculated within the cluster model. The dotted blue curves show the difference between the experimental data (thick black line) and the red curve. Fit parameters for $E \parallel c$ are $U_{\text{mol}} = 0.5$ eV and $t(\text{b1}) = 0.21$ eV. The vibrational frequencies ν_i and respective coupling constants Q_i are: $\nu_4 = 1460 \text{ cm}^{-1}$ $Q_4 = 610$, $\nu_6 = 1287 \text{ cm}^{-1}$ $Q_6 = 95$, $\nu_{10} = 878 \text{ cm}^{-1}$ $Q_{10} = 120$, and $\nu_{13} = 445 \text{ cm}^{-1}$ $Q_{13} = 240$. For $E \parallel a$ we used $U_{\text{mol}} = 0.5$ eV and $t(\text{b1}) = 0.19$ eV; the frequencies and coupling constants are the same except $Q_4 = 680$.

transfer between the dimers.

In order to identify the intradimer transition band for polarization $E \parallel a$, we start with the respective parameters obtained for the $E \parallel c$. Only the position of the intradimer charge transfer is varied by changing the transfer integral b1 until the positions of emv-coupled features, which are considerably softer along a axis, match the experiment. Consequently, the position of the intradimer transition follows these emv-coupled vibrations. The fit with $t(\text{b1}) = 0.19$ eV suggests that the L_{dimer} has its maximum at about 2900 cm^{-1} in the a direction, compared to 3300 cm^{-1} found for $E \parallel c$.

For a further analysis of the data focused on itinerant charge carriers, we subtract the results of the cluster-model calculations from the experimental data. As seen in Fig. 12, the remaining intensity of the emv-coupled vibrational modes is small; this confirms that they are only very weakly coupled to charge carriers which are not localized on the dimers. Interestingly, this is only true for the metallic samples with high Br content (85% and

90%). Once we approach the insulating side of the phase diagram (low Br concentration), a charge transfer only in a dimer does not account for all the intensity of the emv-coupled features anymore. These spectra are much closer to those proposed by the tetramer model,⁶² indicating that once the inter-dimer excitations get localized they are also coupled to the totally-symmetric vibrations of BEDT-TTF molecule.

E. Anisotropy of the spectra

One of the striking features of the κ -phase spectra is the anisotropy, which from the first glance one would not expect on an orthorhombic unit cell⁶³ with two crystallographically identical dimers and an angle between the optical axes and the dimers close to 45 degrees. This anisotropy involves the intradimer transition, and above we showed that the cluster model gives a good explanation for the anisotropy in the vibrational features.

It should be noted that the distance between the dimers is different in a and c direction, with some preference along the a axis, as depicted in Fig. 1. In addition, the molecules are not standing upright on the (ac) plane, but considerably tilted in a direction (in an alternating fashion in such a way that adjacent layers form a herring-bone pattern).⁴⁴ The higher reflectivity observed in the $E \parallel a$ polarization in these compounds suggests that a projection of the dipole moment for all the electronic transitions onto this axis is higher.

An explanation for the difference in position and intensity of the intradimer charge transfer band L_{dimer} observed parallel to a and c axes might be given by a so-called Davydov splitting.⁶⁴ In the present case of the κ -salts, the dimers are taken as the principal unit, i.e. a ‘big molecule’ with one hole and spin residing on it. In general, if the unit cell possesses a center of symmetry and two identical molecules in the cell, a Davydov splitting of the intra-molecular electronic transitions between the upper molecular orbitals (intra-molecular excitons, Frenkel excitons) is observed.⁶⁴ In this case two bands which are distinct in position and intensity are expected parallel to the symmetry axes of the unit cell. Applied to the present case, the electronic spectrum exhibits two distinct bands for the two polarizations parallel to the symmetry axes of the unit cell. Thus, the anisotropy of the intradimer transition can be considered as a Davydov splitting of the dimer excitation. Indeed, the less symmetrical (monoclinic) κ -(BEDT-TTF)₂Hg(SCN)₄X ($X = \text{Cl}, \text{Br}$) show less anisotropy of the spectra⁶⁵ than the presented orthorhombic compounds.

F. Allocating the transition between the Hubbard bands

From the analysis presented above, we conclude that the lower-frequency contribution L_{Hubbard} to the mid-

infrared band originates from excitations across the Mott-Hubbard gap which allows us to determine the effective Coulomb repulsion U_{eff} to be approximately 2200 cm^{-1} . This assignment is supported by comparing our data to spectra of the superconductor κ -(BEDT-TSeF)₄Hg_{2.89}Br₈. The replacement of the four inner sulphur atoms with selenium reduces the on-site Coulomb repulsion but increases the transfer integrals to neighboring molecules. Therefore, the BEDT-TSeF-based analogs are much closer to the normal metallic state; the contributions of itinerant and localized charge carriers are well separated in the optical spectra. It has clearly been observed⁵⁵ that with decreasing temperatures the contribution of the electrons in the conduction band (Drude-peak and transitions between Hubbard bands) shifts to lower frequencies while there is a blue shift of the excitations of the localized charge carriers, similar to the metallic compounds studied in this work.

Calculations by Merino and McKenzie⁶⁶ reveal that in strongly correlated metals the coupling between electrons and phonons leads to a non-monotonic temperature dependence of the vibrational modes near the coherence temperature T_{coh} . The shift is most pronounced (up to 5%) for phonons in the energy range comparable to $U_{\text{eff}}/2$, and becomes weaker for larger or smaller frequencies. Raman measurements perfectly agree with these predictions.⁶⁷ Evidently, the situation is more complicated for infrared data, as the vibrations are activated only by emv-coupling and influence in frequency and intensity by the charge excitations within the dimers. Nevertheless, this electron-phonon coupling might be an explanation for a softening of $\nu_4(A_g)$ and $\nu_6(A_g)$ below $T_{\text{coh}} \approx 50 \text{ K}$ for the compounds κ -(BEDT-TTF)₂Cu[N(CN)₂]Br_{*x*}Cl_{1-*x*} with $x = 0\%$ and 40% where the electronic correlations U/t are strongest. A close inspection reveals that the higher frequency mode $\nu_{45}(B_{2u})$ exhibits a similar behavior for the insulating samples with low Br content, but weaker; while no change is observed for the far-infrared vibration $\nu_{14}(A_g)$. This also suggests that the effective Coulomb repulsion U_{eff} is of the order of 2000 to 2500 cm^{-1} .

V. CONCLUSION

Our comprehensive analysis of the temperature- and Br-concentration dependence of mid-infrared

and emv-coupled features in κ -(BEDT-TTF)₂-Cu[N(CN)₂]Br_{*x*}Cl_{1-*x*} allows us to distinguish two contributions in the mid-infrared part of the spectra. This interpretation is supported by the calculations which describe a charge transfer in a dimer and its coupling to the totally symmetric vibrations of BEDT-TTF molecule. The higher frequency L_{dimer} band (3300 cm^{-1} for the polarization $E \parallel c$ and presumably around 2900 cm^{-1} for $E \parallel a$) originates from the charge transfer between the BEDT-TTF molecules in dimers. This charge-transfer within the dimers is coupled to the intramolecular vibrations of BEDT-TTF and is responsible for the major part of the emv-coupled features intensity for the metallic compounds, while in the insulating materials the lower-frequency contribution is presumably also coupled with vibrations. The lower-frequency contribution to the mid-infrared band L_{Hubbard} located at 2200 cm^{-1} is isotropic and assigned to transition between two Hubbard bands which form due to strong electronic correlations. In Part II the dynamical properties of the itinerant charge carriers will be analyzed and discussed in detail, including extensive calculations by dynamical mean-field-theory.

VI. ACKNOWLEDGMENTS

The authors are grateful to Alain Barreau for his help at the microscopic characterization of the sample concentrations. Belal Salameh performed the dc measurements. We acknowledge the helpful discussions with Jaime Merino and Ross McKenzie, who initiated the study many years ago, and A. Girlando, M. Masino, and A. Painelli. The project was partially supported by the Deutsche Forschungsgemeinschaft (DFG). ND is grateful to the Alexander von Humboldt-Foundation for the continuous support. B.P., V.S. and R.V. thank V. Yartsev for useful discussions and the algorithm of calculations by a cluster model.

* Electronic address: dressel@pi1.physik.uni-stuttgart.de

¹ D. Jérôme, in: *Organic Conductors*, edited by J.-P. Farges (Marcel Dekker, New York, 1994), p. 405.

² T. Ishiguro, K. Yamaji, and G. Saito, *Organic Superconductors*, 2nd edition (Springer-Verlag, Berlin, 1998).

³ R.H. McKenzie, *Science*, **278**, 821 (1997).

⁴ H. Seo, C. Hotta, H. Fukuyama, *Chem. Rev.* **104**, 5005 (2004).

⁵ M. Dressel and N. Drichko, *Chem. Rev.* **104**, 5689 (2004).

⁶ T. Mori, H. Mori, and S. Tanaka, *Bull. Chem. Soc. Jpn.* **72**, 179 (1999).

⁷ By now, the observations are not completely understood: the coupling between the layers is certainly crucial, however, simple volume effects cannot explain the behavior.

⁸ A. Georges, G. Kotliar, W. Krauth, and M.J. Rozenberg, *Rev. Mod. Phys.* **68**, 13 (1996).

- ⁹ J. Merino and R. H. McKenzie, Phys. Rev. B **61**, 7996 (2000).
- ¹⁰ M. Lang and J. Müller, *Organic Superconductors*, in: *The Physics of Superconductors*, Vol. 2, edited by K.H. Bennemann and J.B. Ketterson (Springer-Verlag, Berlin, 2004), p. 453.
- ¹¹ K. Miyagawa, A. Kawamoto, and K. Kanoda, Phys. Rev. Lett. **89**, 017003 (2002).
- ¹² S. Lefebvre, P. Wzietek, S. Brown, C. Bourbonnais, D. Jérôme, C. Mezière, M. Fourmigué, and P. Batail, Phys. Rev. Lett. **85**, 5420 (2000).
- ¹³ P. Limelette, P. Wzietek, S. Florens, A. Georges, T.A. Costi, C. Pasquier, D. Jérôme, C. Mezière, and P. Batail, Phys. Rev. Lett. **91**, 016401 (2003).
- ¹⁴ F. Kagawa, T. Itou, K. Miyagawa, and K. Kanoda, Phys. Rev. B **69**, 064511 (2004); F. Kagawa, T. Itou, K. Miyagawa, and K. Kanoda, Phys. Rev. Lett. **93**, 127001 (2004); F. Kagawa, K. Miyagawa, and K. Kanoda, Nature **436**, 534 (2005).
- ¹⁵ J. E. Eldridge, K. Kornelsen, H. H. Wang, J. M. Williams, A. V. D. Crouch, and D. M. Watkins, Solid State Commun. **79**, 583 (1991).
- ¹⁶ M. Tamura, H. Tajima, K. Yakushi, H. Kuroda, A. Kobayashi, R. Kato, and H. Kobayashi, J. Phys. Soc. Jpn. **60**, 3861 (1991).
- ¹⁷ K. Kornelsen, J. E. Eldridge, H. H. Wang, H. A. Charlier, and J. M. Williams, Solid State Commun. **81**, 343 (1992).
- ¹⁸ J.E. Eldridge, Y. Xie, H.H. Wang, J.M. Williams, A.M. Kini, and J.A. Schlueter, Spectrochim. Acta A **52**, 45 (1996); *idem*, Mol. Cryst. Liq. Cryst. **284**, 97 (1996).
- ¹⁹ R.M. Vlasova, O.O. Drozdova, V.N. Semkin, N.D. Kushch, and E.B. Yagubskii, Phys. Solid State **38**, 481 (1996).
- ²⁰ J.J. McGuire, T. Rööm, A. Pronin, T. Timusk, J.A. Schlueter, M.E. Kelly, and A.M. Kini, Phys. Rev. B **64**, 094503 (2001).
- ²¹ T. Sasaki, I. Ito, N. Yoneyama, N. Kobayashi, N. Hanasaki, H. Tajima, T. Ito, and Y. Iwasa, Phys. Rev. B **69**, 064508 (2004).
- ²² The optical study of an alloy κ -(BEDT-TTF)₂Cu[N(CN)₂]Br_{0.5}Cl_{0.5} was performed in mid-infrared and could not give an information about presence or absence of a Drude-peak.
- ²³ R.M. Vlasova, O.O. Drozdova, V.N. Semkin, N.D. Kushch, and E.B. Yagubskii, Phys. Solid State **35**, 408 (1993).
- ²⁴ O.O. Drozdova, V.N. Semkin, R.M. Vlasova, N.D. Kushch, and E.B. Yagubskii, Synthetic Metals **64**, 17 (1994).
- ²⁵ B.V. Petrov, V.N. Semkin, R.M. Vlasova, V.M. Yartsev, N.D. Kushch, and A. Graja, in: *Molecular Low-Dimensional and Nanostructured Materials for Advanced Applications*, edited by A. Graja et al. (Kluwer Academic Publ., Dordrecht, 2002), p. 259.
- ²⁶ K.D. Troung, B. Danilovic, D. Achkir, S. Jandl, and M. Poirier, Synth. Met. **85**, 1577 (1997).
- ²⁷ M. Dumm, D. Faltermeier, N. Drichko, M. Dressel, C. Mezière, P. Batail, J. Merino, and R. McKenzie, *to be published*.
- ²⁸ D. Schweitzer, private communication.
- ²⁹ The small size of the crystals limited our possibility of low-frequency measurements. In the case of the $x = 40\%$ sample, the crystal was so tiny, that the measurements in the FIR range were only possible without a polarizer due to the weak signal. Since the anisotropy of the spectra in the FIR range is low, it was possible to use the data for both polarizations.
- ³⁰ The pure compound κ -(BEDT-TTF)₂Cu[N(CN)₂]Cl follows the rise in $\rho(T)$ down to about 30 K, at lower temperatures the resistivity levels off at a value of approximately $10^3 \Omega\text{cm}$ and even shows a slight drop around $T = 10$ K. This behavior is well documented in literature^{31,32,33} and associated with traces of superconductivity induced by internal stress or surface effects. Similar effects are seen in samples with very low Br content $x = 15\%$.³⁴
- ³¹ J.M. Williams, A.M. Kini, H.H. Wang, K.D. Carlson, U. Geiser, L.K. Montgomery, G.J. Pyrka, D.M. Watkins, J.M. Komers, S.J. Boryschuk, A.V. Strieby Crouch, W.K. Kwok, J.E. Schierber, D.L. Overmyer, D. Yung, and M.H. Whangbo, Inorg. Chem. **29**, 3271 (1990); H.H. Wang, K.D. Carlson, U. Geiser, A.M. Kini, A.J. Schultz, J.M. Williams, L.K. Montgomery, W.K. Kwok, U. Welp, K.G. Vander voort, S.J. Boryschuk, A.V. Strieby Crouch, J.M. Komers, D.M. Watkins, J.E. Schierber, D.L. Overmyer, D. Yung, J.J. Novoa, and M.H. Whangbo, Synth. Met. **41-43**, 1983 (1991).
- ³² H. Ito, T. Ishiguro, M. Kubota, and G. Saito, J. Phys. Soc. Jpn. **65**, 2987 (1996).
- ³³ H. Kobayashi, A. Miyamoto, T. Naito, R. Kato, A. Kobayashi, and J.M. Williams, Chem. Lett. 1997 (1991).
- ³⁴ V.A. Bondarenko, Yu.V. Sushko, V.I. Barchuk, V.S. Yefanov, V.V. Dyakin, M.A. Tanatar, N.D. Kushch, and E.B. Yagubskii, Synth. Met. **56**, 2386 (1993); Yu.V. Sushko, K. Andres, N.D. Kusch, and E.B. Yagubskii, Solid State Commun. **87**, 589 (1993); Yu.V. Sushko, T. Ishiguro, K. Andres, S. Horiuchi, G. Saito, N.D. Kushch, and E.B. Yagubskii, J. Supercond. **7**, 937 (1994); H. Posselt, H. Müller, K. Andres, Yu.V. Sushko, and G. Saito, Synth. Met. **70**, 917 (1995).
- ³⁵ C.C. Homes, M. Reedyk, D.A. Cradles, and T. Timusk, Applied Optics **32**, 2976 (1993).
- ³⁶ M. Dressel and G. Grüner, *Electrodynamics of Solids* (Cambridge University Press, Cambridge, 2002).
- ³⁷ K. Kornelsen, J. E. Eldridge, H. H. Wang, and J. M. Williams, Phys. Rev. B **44**, 5235 (1992).
- ³⁸ J.E. Eldridge, C.C. Homes, H.H. Wang, A.M. Kini, and J.M. Williams, Spectrochim. Acta A **51**, 947 (1995).
- ³⁹ J.E. Eldridge, Y. Xie, Y. Lin, C.C. Homes, H.H. Wang, J.M. Williams, A.M. Kini, and J.A. Schlueter, Spectrochim. Acta A **53**, 565 (1997).
- ⁴⁰ Previously, the assignment of the modes was done assuming D_{2h} symmetry of the BEDT-TTF molecule (plane BEDT-TTF molecule).^{5,17,18,38,39,41} By now the general agreement is that the molecules in κ -(BEDT-TTF)₂Cu(NCS)₂ only have D_2 due to the twisted ethylene groups^{42,43,44} leading to 19 A_1 totally symmetric modes. For the κ -(BEDT-TTF)₂Cu[N(CN)₂]Br and κ -(BEDT-TTF)₂Cu[N(CN)₂]Cl-family the molecules are eclipsed and exhibit only C_{2h} symmetry, as recently pointed out in Ref. 45.
- ⁴¹ M.E. Kozlov, P.I. Pokhodnia, and A.A. Yurchenko, Spectrochim. Acta A **43**, 323 (1987); M.E. Kozlov, P.I. Pokhodnia, and A.A. Yurchenko, Spectrochim. Acta A **45**, 437 (1989).
- ⁴² M. Meneghetti, R. Bozio, and C. Pecile, J. Phys. I (France) **47**, 1377 (1986); Synth. Met. **19**, 143 (1987).
- ⁴³ A. Girlando, M. Masino, A. Brillante, R.G. Della Valle, and E. Venuti, to be published in: *Horizons in Superconductivity Research* (Nova Science Publisheres, New York, 2004).
- ⁴⁴ J. M. Williams, J. R. Ferraro, R. J. Thorn, K. D. Carlson,

- U. Geiser, H. H. Wang, A. M. Kini, and M. H. Whangbo, *Organic Superconductors* (Prentice Hall, Englewood Cliffs NJ, 1992).
- ⁴⁵ R. Wesolowski, J.T. Haraldsen, J. Cao, J.L. Musfeldt, I. Olejniczak, J. Choi, Y.J. Wang, and J.A. Schlueter, *Phys. Rev. B* **71**, 214514 (2005).
- ⁴⁶ T. Sugano, H. Hayashi, M. Kinoshita, and K. Nishikida, *Phys. Rev. B* **39**, 11387 (1989).
- ⁴⁷ M.J. Rozenberg, G. Kotliar, H. Kajueter, G.A. Thomas, D.H. Rapkine, J.M. Honig, and P. Metcalf, *Phys. Rev. Lett.* **75**, 105 (1995); M.J. Rozenberg, G. Kotliar, H. Kajueter, *Phys. Rev. B* **54**, 8452 (1996).
- ⁴⁸ R.H. McKenzie, *Comments Cond. Mat.* **18**, 309 (1998).
- ⁴⁹ D. Jung, M. Evain, J.J. Novoa, M.H. Whangbo, M.A. Beno, A.M. Kini, A.J. Schultz, J.M. Williams and P.J. Nigrey, *Inorg. Chem.* **28**, 4516 (1989).
- ⁵⁰ U. Geiser, A.J. Schultz, H.H. Wang, D.M. Watkins, D.L. Stupka, J.M. Williams, J.E. Schirber, D.L. Overmyer, D. Jung, J.J. Novoa and M.H. Whangbo, *Physica C* **174**, 475 (1991).
- ⁵¹ H. Kino and H. Fukuyama, *J. Phys. Soc. Jpn.* **64**, 2726 (1995); *ibid.* **64**, 4523 (1995); *ibid.* **65**, 2158 (1996).
- ⁵² K. Kanoda, *Hyperfine Interact.* **104**, 235 (1997).
- ⁵³ A. Fortunelli and A. Painelli, *Phys. Rev. B* **55**, 16088 (1997).
- ⁵⁴ By comparing the effects of ‘chemical’ and hydrostatic pressure, Mori *et al.*⁶ point out that the application of the hydrostatic pressure (but also thermal contraction) to the Cl compound reduces the b1/p ratio, leading a less correlated state.
- ⁵⁵ N. Drichko, B. Petrov, V.N. Semkin, R.M. Vlasova, O.A. Bogdanova, E.I. Zhilyaeva, R.N. Lyuboskaya, I. Olejniczak, H. Kobayashi, and A. Kobayashi, *J. Phys. IV (France)* **114**, 305 (2004); R.M. Vlasova, N.V. Drichko, B.V. Petrov, V.N. Semkin, E.I. Zhilyaeva, R.N. Lyuboskaya, I. Olejniczak, A. Kobayashi, and H. Kobayashi, *Phys. Solid State* **46**, 1985 (2004).
- ⁵⁶ As discussed in the following paragraph, the ν_4 mode appears as a double peak due to the ν_6 antiresonance. We fit the complete feature by a Lorentzian and choose the center frequency, while commonly the upper peak is listed as the ν_4 frequency.
- ⁵⁷ M.J. Rice, *Phys. Rev. Lett.* **37**, 36 (1976).
- ⁵⁸ V.M. Yartsev, O.O. Drozdova, V.N. Semkin and R.M. Vlasova, *J. Phys. I (France)* **6**, 1673 (1996); V.M. Yartsev, in: *Materials and Measurements in Molecular Electronics*, ed. by K. Kajimura and S. Kanoda (Springer-Verlag, Berlin 1996), p. 189; V. M. Yartsev and A. Graja, *Int. Journ. of Mod. Phys. B*, **12**, 1643 (1998).
- ⁵⁹ Delhaes P., Yartsev V.M., *Advances in Spectroscopy*, **22**, R.J.H. Clark, R.E. Hester Eds. *John Wiley and Sons*, 1993, 199. V. M. Yartsev, O. Fichet, J.-P. Borgion and P. Delhaes. *J. Phys. II France* **3**, 647 (1993).
- ⁶⁰ M. Meneghetti, *Phys. Rev. B* **44**, 8554 (1991).
- ⁶¹ G. Visentini, M. Masino, C. Bellitto, and A. Girlando, *Phys. Rev. B* **58**, 9460 (1998).
- ⁶² R.M. Vlasova, S.Ya. Prie, V.N. Semkin, R.N. Lyuboskaya, E.I. Zhilyaeva, E.B. Yagubskii, and V.M. Yartsev, *Synth. Met.* **48**, 129 (1992).
- ⁶³ The dihedral angle is about 92° which makes the charge transfer between the dimer contribute stronger in the c direction.
- ⁶⁴ A.S. Davydov, *Theory of Molecular Excitons* (Plenum, New York, 1971).
- ⁶⁵ R.M. Vlasova, N.V. Drichko, O.O. Drozdova, and R.N. Lyubovskaya, *Phys. Solid State* **39**, 1165 (1997).
- ⁶⁶ J. Merino and R. H. McKenzie, *Phys. Rev. B* **62**, 16442 (2000).
- ⁶⁷ Y. Lin, J.E. Eldridge, H.H. Wang, A.M. Kini, M.E. Kelly, J.M. Williams, and J.A. Schlueter, *Phys. Rev. B* **58**, R599 (1998).